for by degassing of CO_2 to the atmosphere and by downward flux of sinking particles. Estimates of the partitioning between these latter two processes can be made using the downward flux of organic nitrogen as a measure of the downward export of organic carbon. In order to estimate downward flux of nitrogen, and because concurrent measurements of TOC, DIC and TON near the Equator were few, we first estimated the amount of nitrogen that accumulated in the suspended organic fraction. TON concentrations were estimated from TOC concentrations measured during the OACES program by assuming a C:N atomic ratio of 12 for total organic matter, a value reported for the surface layer along 110° W (ref. 10). Measured DIC concentrations were then plotted against estimated concentrations of total nitrogen (TIN plus estimated TON; Fig. 2c; s.e. of slope, 0.57). A decrease in total nitrogen of 8 μM corresponded to a 99.4 μmol kg^{-1} decrease in DIC concentrations. The organic carbon removed to depth with the nitrogen was estimated using a C:N atomic ratio for sinking particles of 6.6. The downward flux of organic carbon represented 52.8 μmol kg^{-1} (53%) of the total DIC drawdown of 99.4 μmol kg^{-1}. This analysis indicates that <6% and 53% of DIC depletion occurred owing to the production of TOC (with the potential for horizontal export by advection from upwelling system) and downward flux of sinking particles, respectively. Mass balance requires that the remaining 41% of inorganic carbon loss take place by degassing of CO_2 to the atmosphere.

TOC production and accumulation in the surface layer accounted for ~10% of the net community production (sum of TOC accumulation and downward flux of sinking particles) of carbon, compared to approximately 27% for nitrogen. If these data sets were directly comparable, we would expect the fractional accumulation of organic carbon in the surface layer to be greater than that for organic nitrogen. This follows from the high C:N ratio of the material. Such an inconsistency suggests that a direct comparison of the data sets is not warranted, perhaps due to analytical uncertainties and natural variability in the equatorial system.

Sensitivity analysis for the C:N ratios for sinking particles demonstrates that the proportion of C found in the TOC pool remains the same, while the contributions of export by degassing and sinking particles varies. By assuming a higher C:N ratio for sinking particles of 9, this contribution to export increases to 72%.

Assessing the fate of carbon fixed by new production is critical for determining the role of the biological pump in the long-term removal of carbon from the surface ocean. Sinking particles can remove organic carbon to below the main thermocline, thereby sequestering the carbon for periods approaching the timescale of oceanic turnover (10^2–10^4 years). Horizontal export of organic matter from the upwelling regions in the equatorial Pacific Ocean results in negligible removal of carbon from the surface ocean, leaving it available for export to the atmosphere on short timescales. The results presented here demonstrate that vertical processes (carbon transfer by degassing to the atmosphere and by downward flux of biogenic particles to the deep ocean) predominate in the export of carbon from this globally important region. □

Received 20 June 1996; accepted 13 January 1997.

1. Murray, J. W., Barber, R. T., Roman, M. R., Bacon, M. P. & Feely, R. A. *Science* **266,** 58–65 (1994).
2. Feely, R. A. *et al. J. Geophys. Res.* **92,** 6545–6558 (1987).
3. Francey, R. J. *et al. Nature* **373,** 326–330 (1995).
4. Wong, C. S., Chan, Y. H., Page, J. S., Smith, G. E. & Bellegay, R. D. *Tellus* **45,** 64–79 (1993).
5. Tans, P. P., Fung, I. Y. & Takahashi, T. *Science* **247,** 1431–1438 (1990).
6. Chavez, F. P. & Barber, R. T. *Deep-Sea Res.* **34,** 1229–1243 (1987).
7. Feely, R. A. *et al. Deep-Sea Res. II* **42,** 365–386 (1995).
8. Peltzer, E. T. & Hayward, N. A. *Deep-Sea Res. II* **43,** 1155–1180 (1996).
9. Libby, P. S. & Wheeler, P. A. *Deep-Sea Res. I* (in the press).
10. Hansell, D. A. & Waterhouse, T. Y. *Deep-Sea Res. I* (in the press).
11. Lamb, M. F. *et al. Data Rep. ERL PMEL-56* (NOAA, Seattle, WA, 1995).
12. Lukas, R. & Lundstrom, E. *J. Geophys. Res.* **96,** 3343–3357 (1991).
13. Wanninkhof, R. *et al. Deep-Sea Res. II* **42,** 387–409 (1995).
14. Redfield, A. C., Ketchum, B. H. & Richards, F. A. in *The Sea* Vol. 2 (ed. Hill, M. N.) 26–77 (Wiley, New York, 1963).

Acknowledgements. We thank R. Feely, M. Roberts, E. Peltzer, S. Libby and P. Wheeler for their analytical work, and whose data we used in the analysis. Comments from R. Murnane were appreciated.

Correspondence should be addressed to D.A.H. (e-mail: dennis@bbsr.edu).

GPS measurements of present-day convergence across the Nepal Himalaya

Roger Bilham*, Kristine Larson†, Jeffrey Freymueller‡ & Project Idylhim members§

* *CIRES and Department of Geological Sciences, University of Colorado, Boulder, Colorado 80309, USA*
† *Department of Aerospace Engineering Sciences, University of Colorado, Boulder, Colorado 80309, USA*
‡ *Geophysical Institute, University of Alaska, Fairbanks, Alaska 99775, USA*

The high elevations of the Himalaya and Tibet result from the continuing collision between India and Asia, which started more than 60 million years ago[1–4]. From geological and seismic studies of the slip rate of faults in Asia[5], it is believed that approximately one-third of the present-day convergence rate between India and Asia (58 ± 4 mm yr^{-1}) is responsible for the shortening, uplift and moderate seismicity of the Himalaya. Great earthquakes also occur infrequently in this region, releasing in minutes the elastic strain accumulated near the boundary zone over several centuries, and accounting for most of the advance of the Himalaya over the plains of India. The recurrence time for these great earthquakes is determined by the rate of slip of India beneath Tibet, which has hitherto been estimated indirectly from global plate motions[6], from the slip rates of faults in Asia[7,8], from seismic productivity[9], and from the advance of sediments on the northern Ganges plain[10]. Here we report geodetic measurements, using the Global Positioning System (GPS), of the rate of contraction across the Himalaya, which we find to be 17.52 ± 2 mm yr^{-1}. From the form of the deformation field, we estimate the rate of slip of India beneath Tibet to be 20.5 ± 2 mm yr^{-1}. Strain sufficient to drive one or more great Himalayan earthquakes, with slip similar to that accompanying the magnitude 8.1 Bihar/Nepal 1934 earthquake, may currently be available in western Nepal.

In March 1991 we used Global Positioning System (GPS) geodesy to measure the relative positions of 24 points in India, Nepal and Tibet. Some of these points were remeasured in 1992[11] and in 1995, and additional points were installed in November 1995 in collaborative programmes between US, Nepalese, Indian, Chinese and French teams. Data were obtained in five 8-h sessions in 1991 and 1992 and for three to five consecutive 24-h sessions in 1995. We occupied a central point near Kathmandu (NAGA) continuously during each survey relative to which all positions are referred. The data from all surveys were analysed with the GIPSY software[12], using an estimation strategy summarized in ref. 13, and orbital data from the global tracking network using a geodetic reference frame defined by ITRF94 (ref. 14).

For 20 points common to the 1994 and 1991 surveys the mean formal uncertainty in northward velocities relative to NAGA is ±1.1 mm yr^{-1}, and ±1.8 mm yr^{-1} for eastward components, considerably smaller than previous GPS measurements in the Himalaya[15]. The maximum observed convergence velocity between northern India and southern Tibet is 18.2 ± 2 mm yr^{-1} at 13° ± 4°. Mean velocity uncertainties relative to Bangalore, southern India (the nearest permanent site), are ±1.9 mm yr^{-1} north and ±2.3 mm yr^{-1} east (Fig. 1). In southern Nepal, convergence velocities

§ F. Jouanne (Univ. Savoie, Chambiry, France), P. Le Fort, P. Leturmy & J. L. Mugnier (LGCA-CNRS, UJF, Grenoble, France), J. F. Gamond, J. P. Glot & J. Martinod, (LGIT-CNRS, UJF, Grenoble, France), N. L. Chaudury, G. R. Chitrakar, U. P. Gautam, B. P. Koirala, M. R. Pandey, R. Ranabhat, S. N. Sapkota, P. L. Shrestha, M. C. Thakuri, U. R. Timilsina & D. R. Tiwari (Dept Mines and Geology, Kathmandu, Nepal), G. Vidal (ENS Lyon, France), C. Vigny (ENS Paris, France), A. Galy (CRPG-CNRS, Nancy, France), B. de Voogd (Univ. Pau, France).

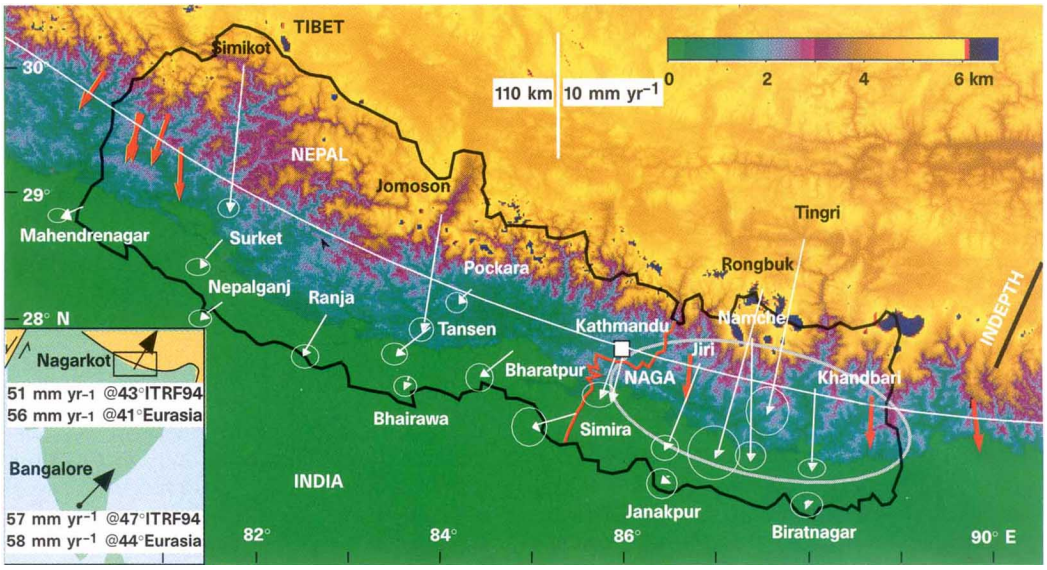

Figure 1 Himalayan GPS velocity vectors (white lines with arrowheads) 1991–95 relative to Bangalore. The levelling line (see text; red) passes near Nagarkot (white square, NAGA, to which GPS processing was referenced) and the western edge of the inferred rupture of the 1934 earthquake (large ellipse). White line, small-circle approximation for the Himalayan arc; black line, INDEPTH seismic profile[26]; red arrows, slip vectors for moderate earthquakes[15] since 1960. Inset, location map showing Bangalore and Nagarkot vectors[18,19] for ITRF94 and for a no-net-rotation frame for Eurasia fixed with uncertainties of 4 mm in scale and 5° in azimuth. Error ellipses are one standard deviation; the colour scale indicates elevation in kilometres.

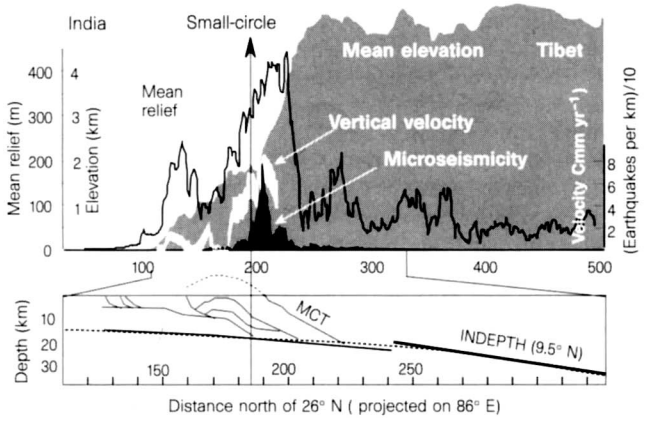

Figure 2 Top, levelling data (white envelope), seismic data[28] (black envelope), mean elevation data (shaded) and topographic relief (0.05° digital terrain data) at 86° ± 1° E. The high peaks of the Himalaya are found close to the edge of the Tibetan plateau, 20–30 km north of the region of maximum relief. A small-circle fit to maximum Himalayan stream gradients and moderate seismicity[24] intersects the section near maximum downslope tilts (2.5 μrad yr^{-1}) in the vertical velocity field. Bottom, a typical geological section for eastern Nepal[25] (MCT, Main Central Thrust) and the estimated dip of the upper surface of the Indian plate from the INDEPTH seismic profile[26] (see Fig. 1), using the small-circle approximation for the Himalayan arc to project at 86° E. Dashed line, polynomial fit used to approximate flexure of the Indian plate used in Fig. 3.

are low but approximately arc-normal. In contrast, the mean convergence velocity for points on the southern margin of the Tibetan plateau is apparently directed at the approaching Indian plate (17° ± 4°), arc-normal in eastern Nepal but trending 22° east of arc-normal in western Nepal, not significantly different from the slip vectors of published focal mechanisms for nearby thrust earthquakes[16]. Focal mechanisms for moderate earthquakes along the Himalayan arc approximate arc-normal slip which, if India is assumed rigid, requires ~N100° E extension of the southern Tibetan plateau at a rate approximating the rate at which India collides with Tibet[17–19]. Thus if extension occurs steadily, Simikot and Tingri should recede from each other at ~7 ± 2 mm yr^{-1}. That these points currently converge at 3 ± 3 mm yr^{-1} requires episodic and/or heterogeneous east–west extension of southern Tibet.

GPS data from NAGA and Bangalore were used recently to confirm[20] the NUVEL1 hypothesis that India rotates anticlockwise relative to the Australia plate[6]. The data we have since collected at Bangalore confirm NUVEL1 motions in southern India, but it is clear that NAGA, which approaches Bangalore at 5.0 ± 1.5 mm yr^{-1}, is within the deforming zone between India and Eurasia, consistent with earlier findings that minor deformation occurs in the Lesser Himalaya[21]. The eastward motion of our points in Nepal and south central Tibet relative to Eurasia, assuming no net rotation of India and Eurasia, is 25 ± 5 mm yr^{-1}.

Because we may have incompletely sampled deformation in southern Tibet, our GPS data do not provide an upper bound to the rate at which India slips beneath Tibet. But, if we assume that the slip of India beneath Tibet can be approximated by slip on a subsurface dislocation (a mathematically convenient but by no means unique explanation for surface deformation), a strong constraint occurs because the maximum uplift rate in the vertical velocity field, and the maximum gradient in the horizontal velocity field, overlie the tip of an active subsurface dislocation[22,23]. Moreover, if the dip of the dislocation is shallow (<15°) the horizontal deformation field is approximately antisymmetric about the tip of this dislocation, permitting data from the south of the dislocation to yield approximate constrains on deformation to its north.

Vertical uncertainties in the GPS data are large (>5 mm yr^{-1}), partly due to uncertainties in the phase centres of some of the antennas used, and these data are inadequate to constrain models of subsurface deformation. Recent spirit-levelling data (Fig. 2) obtained by the Nepalese Survey Department (1977–95), however, confirm a previously identified 40-km wavelength region of uplift in northern Nepal rising at a peak rate of 7 ± 3 mm yr^{-1} relative to the

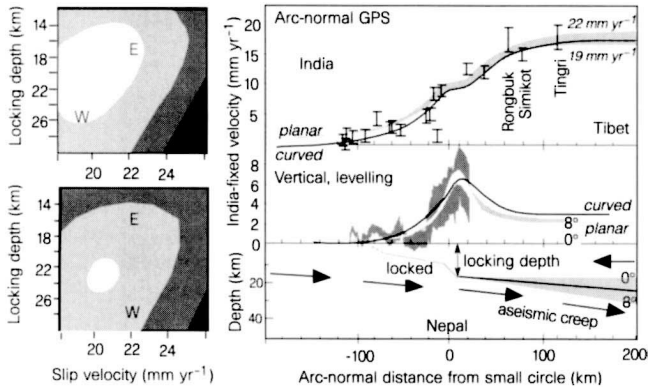

Figure 3 Right, surface deformation resulting from subsurface creep on planar and curved dislocations compared to GPS horizontal velocities and levelling data. Left, shaded regions correspond to 68%, 90% and 99% confidence intervals that satisfy synthetic and observed deformation for a planar dislocation dipping 4° northwards (upper left) and for a curved dislocation (lower left) steepening from 3° northwards at the locking depth to 9° northwards beneath southern Tibet. A deeper locking depth in western Nepal (W) than in eastern Nepal (E) is indicated by the GPS data (68% confidence open ellipses, left) if constraints from the vertical data are ignored.

Indian border. Interestingly, the location of peak uplift corresponds to a maximum in arc-normal Himalayan relief (Fig. 2). The central segment of the Himalayan arc follows a 1,696-km-radius small-circle defined by a belt of moderate Himalayan earthquakes and maximum river gradients[24] which intersects the levelling line ~15 km south of this peak uplift. The similarity in wavelength of the mean arc-normal relief and vertical deformation field, and the correspondence between maximum southward tilt (2.5 μrad yr^{-1}) and maximum stream gradients, suggests that the deformation field we observe is not a transient feature of Himalayan uplift as we might suspect from the brief 18-yr duration of these interseismic measurements. One of several mechanisms that could account for the observed coincidence is that the region may be repeatedly taken close to its elastic limit, with average uplift equal to half its pre-seismic peak value of 2–5 m (assuming 7 ± 3 mm yr^{-1} for, say, 300–500 yr). If a fraction of this uplift were non-recoverable inelastic deformation, permanent uplift of the region would mimic the form of the interseismic deformation field.

To reconcile the levelling data with the GPS data we projected both onto a cross-section parallel to the mean convergence direction at 86° E, using the above small-circle approximation to correct for the curvature of the Himalaya (Fig. 1). The projected horizontal and vertical deformation data were then compared to the surface deformation accompanying slip on a planar dislocation (the simplest of possible slip geometries) locked below, and south of, the region of maximum uplift. A dislocation dipping at $4° \pm 4°$ to the north best fits the data with a slip rate of 20.5 ± 2 mm yr^{-1} and a locking depth of 20 ± 4 km (Fig. 3). When the vertical deformation data are ignored, independent best fits to the GPS data from eastern Nepal favour slip at 22 ± 3 mm yr^{-1} starting at 17 ± 4 km depth dipping to the north at $4° \pm 4°$, but the data from western Nepal require deeper locking depths (24 ± 4 km). Whereas slip on a curved dislocation surface dipping increasingly to the north (approximating the flexure of a descending Indian plate) is permitted by the data, we can exclude the possibility of active creep on dislocations at 10–20 km depths dipping to the north at 10°–30°, on which moderate seismicity has been observed in the past century. Satisfactory models for a curved dislocation have a slip velocity of 20.5 ± 1 mm yr^{-1} and starting dip of $4° \pm 2°$ to the north (compare ref. 25) at a locking depth of 21 ± 2 km, and increase smoothly in dip to 9° northward at a distance of 150 km north of the locking depth (compare ref. 26).

More complex geometries and slip distributions, such as those as have been proposed to explain the vertical velocity data[21] cannot be constrained uniquely by our sparse horizontal GPS data, although we can exclude significant creep on surfaces dipping more than 9° northward. Moreover, convergence south of the Himalayan boundary thrusts in western Nepal (Fig. 1) and its absence in eastern Nepal reveals that deformation is not identical in both regions, indicating spatial and/or temporal variations in the convergence process. Synforms and antiforms with wavelengths of less than 100 km imply along-arc heterogeneity[25,27], but microseismic data in the Himalaya that might assist our identification of active subsurface geometries are insufficiently detailed except for the region near Kathmandu[28]. A deep focus magnitude $M = 6.5$ earthquake occurred in 1988 in southeastern Nepal[29,30] near the southern rupture limit of the great 1934 Bihar/Nepal earthquake. Although this event was too small to produce regionally significant surface deformation, viscoelastic relaxation of the region following the 1934 earthquake may partly be responsible for this event, and for observed differences in deformation style in eastern and western Nepal. Numerical estimates of viscous processes are hindered by incomplete information on the 1934 rupture geometry and slip distribution[31].

The locking depth, an arc-parallel line in our two-dimensional model for sub-Tibetan slip, may correspond to the northern limit of rupture during the great 1934 Bihar/Nepal event. Assuming that rupture does not propagate south of the main frontal thrusts of the southern Himalaya[32], or significantly north of this locking depth, the down-dip width of the 1934 rupture zone is estimated to be less than 90 km. This is 20% shorter than previous estimates, requiring estimates of co-seismic slip and renewal time based on seismic energy release from these events to be increased accordingly. In western Nepal there have been no recent great earthquakes for 200 years and perhaps for much longer. Earthquakes in 1803 (Uttarkashi) and 1833 (Nepal) have been assigned maximum magnitudes of $M = 7.7 \pm 0.2$ based on available historical data[9,33]. Magnitude estimates for earlier events are unavailable, although from readings of colonial and Indian archives it is considered unlikely that a $M > 8$ event beneath the Kumaun Himalaya or western Nepal would have escaped mention in the past 350 years. Hence, one or more great earthquakes in western Nepal, if they occurred today, would release >6 m (refs 33, 34) of co-seismic displacement, similar to other $M > 8$ Himalayan events that have occurred in the past 100 years. □

Received 31 July 1996; accepted 23 January 1997.

1. Molnar, P. *Annu. Rev. Earth Planet. Sci.* **12,** 489–518 (1984).
2. Molnar, P. *J. Himalayan Geol.* **1,** 131–154 (1990).
3. Harrison, M. T., Copeland, P., Kidd, W. S. F. & Yin, A. *Science* **255,** 1663–1670 (1992).
4. Ni, J. F. *Proc. Ind. Acad. Sci. (Earth Planet. Sci.)* **98,** 71–89 (1989).
5. Molnar, P. & Tapponier, P. *Science* **189,** 149–426 (1975).
6. DeMets, C., Gordon, R., Argus, D. & Stein, S. *Geophys. J. Int.* **101,** 425–478 (1990).
7. Molnar, P. & Tapponier, P. *J. Geophys. Res.* **83,** 5361–5375 (1978).
8. Avouac, J.-P. & Tapponier, P. *Geophys. Res. Lett.* **20,** 895–898 (1993).
9. Molnar, P. & Deng, Q. *J. Geophys. Res.* **89,** 6203–6228 (1984).
10. Lyon Caen, H. & Molnar, P. *Tectonics* **4,** 513–518 (1985).
11. Jackson, M. & Bilham, R. *Geophys. Res. Lett.* **21,** 1169–1172 (1994).
12. Lichten, S. M. & Border, J. S. *J. Geophys. Res.* **92,** 12751–12762 (1987).
13. Larson, K. M. & Freymueller, J. *Geophys. Res. Lett.* **22,** 37–40 (1995).
14. Boucher, C., Altamimi, Z., Feissel, M. & Sillard, P. *Results and Analysis of the ITRF94 (IERS Tech. Note 20* IERS Central Bureau, Observatoire de Paris, 1996).
15. Anzidei, M. *Terra Nova* **6,** 82–89 (1994).
16. Molnar, P. & Lyon Caen, H. *Geophys. J. Int.* **99,** 123–153 (1989).
17. Armijo, R., Tapponier, P., Mercier, J. L. & Tonglin, H. *J. Geophys. Res.* **91,** 13803–13872 (1986).
18. England, P. C. & Houseman, G. A. *J. Geophys. Res.* **91,** 3664–3676 (1986).
19. Molnar, P. & Tapponier, P. *Geology* **5,** 212 (1977).
20. Freymueller, J. *et al. Geophys. Res. Lett.* **23,** 3107–3110 (1996).
21. Jackson, M. & Bilham, R. *J. Geophys. Res.* **99,** 13897–13912 (1994).
22. Savage, J. C. *J. Geophys. Res.* **88,** 4984–4996 (1983).
23. Okada, Y. *Bull. Seism. Soc. Am.* **75,** 1135–1154 (1985).
24. Seeber, L. & Gornitz, V. *Tectonophysics* **92,** 335–367 (1983).
25. Schelling, D. *Tectonics* **11,** 925–943 (1992).
26. Makovsky, Y., Klemperer, S. L., Liyan, H., Deyuan, L. & Project INDEPTH team *Tectonics* **15,** 997–1005 (1996).
27. Johnson, M. R. W. *Tectonophysics* **239,** 139–147 (1994).
28. Pandey, M. R. *et al. Geophys. Res. Lett.* **22,** 751–754 (1995).
29. Pandey, M. R. & Nicolas, M. (Rep. 2, Dept. Mines and Geology, HMG Nepal, Kathmandu, 1988).

30. Banerjee, S. N. & Chakravarti, P. (eds) *Bihar-Nepal Earthquake 20 August 1988* (Spec. Publ. 31, Geol. Surv. India, Calcutta, 1993).
31. Yu, Tingto thesis, Univ. Colorado (1995).
32. Bilham, R., Bodin, P. & Jackson, M. *J. Nepal. Geol. Soc.* **11,** 73–88 (1995).
33. Khatri, K. N. *Tectonophysics* **138,** 79–92 (1987).
34. Molnar, P. *Ann. Geophys.* **5,** 663–670 (1987).

Acknowledgements. We thank the Survey Department and the Ministry of Mines and Geology, HMG, Nepal, for their participation in the 1991 and 1995 measurements and for their generous contributions of new data. M. Jackson, B. Washburn and P. Molnar made substantial contributions to the initial GPS network. W. Wang, P. Bodin and F. Sigmundsson gathered GPS data in Tibet, and V. Gaur, J. Paul and S. Jade contributed data from India. R. Bürgmann, F. Blume, D. Shelling, P. Molnar, J-P. Avouac and T. Herring provided insights into modelling and interpretation. This work was supported by the US NSF; we thank Trimble Navigation Solarex Corp. and Campbell Scientific Inc. for donations of equipment.

Correspondence should be addressed to R.G.B. (e-mail: bilham@stripe.Colorado.edu).

Confined subsurface microbial communities in Cretaceous rock

Lee R. Krumholz*, James P. McKinley†, Glenn A. Ulrich* & Joseph M. Suflita*

* *Department of Botany and Microbiology, University of Oklahoma, 770 Van Vleet Oval, Norman, Oklahoma 73019, USA*
† *Pacific Northwest National Laboratory, Richland, Washington 99352, USA*

Deep subsurface microbial communities[1] are believed to be supported by organic matter that was either deposited with the formation sediments or which migrated from the surface along groundwater flowpaths. Investigation has therefore focused on the existence of microorganisms in recently deposited or highly permeable sediments[2,3]. Fewer reports have focused on consolidated rocks[4–7]. These findings have often been limited by inadequate tracer methodology or non-sterile sampling techniques. Here we present evidence for the presence of spatially discrete microbial communities in Cretaceous rocks and advance a mechanism for the long-term survival of these subterranean communities. Samples were collected using aseptic methods and sensitive tracers[8]. Our results indicate that the main energy source for these communities is organic material trapped within shales. Microbial activity in shales appears to be greatly reduced, presumably because of their restrictive pore size[9]. However, organic material or its fermentation products could diffuse into adjacent, more permeable sandstones, where microbial activity was much more abundant. This process resulted in the presence of microbial communities at sandstone–shale interfaces. These microorganisms presumably ferment organic matter and carry out sulphate reduction and acetogenesis.

Alternating members of the Cretaceous Mancos (shale) and Dakota (sandstone) formations were drilled and sampled adjacent to Cerro Negro, a volcanic neck in central New Mexico near the village of Seboyeta. Core samples were collected into lexan liners using aqueous and particulate tracers for detection of potential contaminants[9]. The sampled strata represented relatively minor transgressive and regressive episodes within an overall transgressive sequence[10]. Sandstone members represented near-shore (shore face or near-shore bar) depositional environments; shale members represented adjacent, deeper and less energetic, near-shore ('toe-of-slope') environments.

A regional analysis of groundwater composition and hydrology using water from existing wells was conducted in parallel with this work (refs 9, 11, and J.P.McK., unpublished results). Recharge occurred on an upland mesa 10 km to the west and 425 m higher than the sampled well, where the water table was at a depth of 69 m. Cerro Negro groundwaters were sampled by setting downhole packers across sandstone units (shales were non-transmissive and would not yield water) and removing water to the surface using gas-driven Teflon bladder pumps. Dissolved oxygen was below detection ($0.2\,mg\,l^{-1}$) for three sampled sandstone units, and sulphate and sulphide were present at $80–370\,mg\,l^{-1}$ and $8–14\,mg\,l^{-1}$, respectively. The sandstones and shales contained 0.1–2 wt% sulphide minerals (mainly pyrite). Analysis of isotope data for Paguate and Cubero sandstone aquifers indicated an age for these groundwaters of 20,000–30,000 years. Moreover, relatively low levels of Fe(III) were detected in the sediments (data not shown), and the

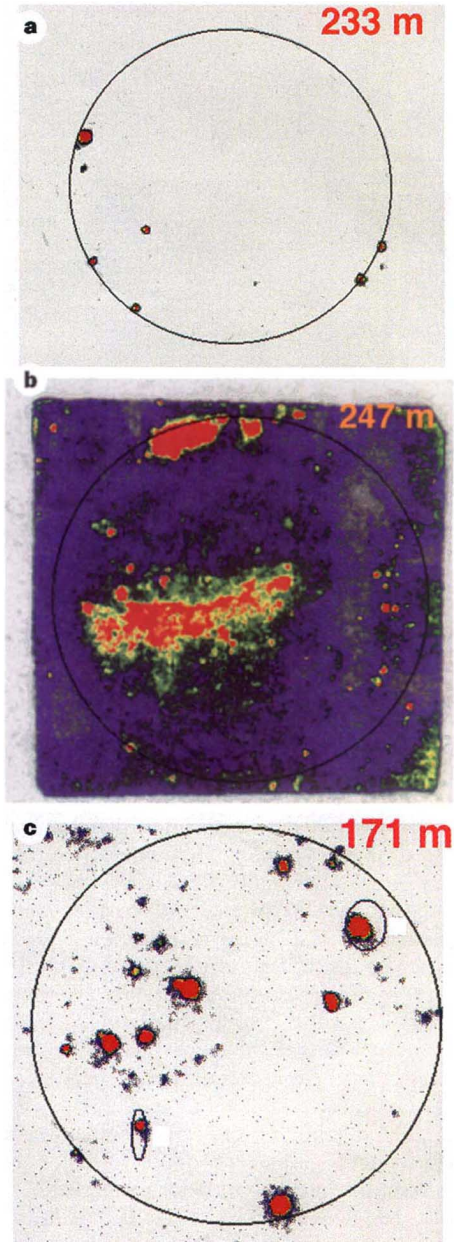

Figure 1 Radioisotope images of sulphate-reduction activity on the freshly exposed face of rock cores obtained from different depths at the Cerro Negro, New Mexico, exploratory drilling site. These images allow for localization of sulphate-reducing activity on a two-dimensional scale. **a**, 233-m core showing microbial contamination of the exterior surface, **b**, 247-m core showing generally high levels throughout, with maximal activity in the centre region. **c**, 171-m core showing patchy distribution of microbial activity. The interior (circled) represents the contact area of the cylindrical core with the foil. The level of radioactivity at that location on the foils is represented in colour (red > yellow > green > blue), although the scale is different for each foil. Small outlined areas in the 171-m core represent points of reference and not necessarily microbial activity.